



Contents lists available at ScienceDirect

Journal of Archaeological Science

journal homepage: www.elsevier.com/locate/jas

Dating (early) modern hearths on a decadal to multi-annual timescale using OSL signals from heated sedimentary quartz

Nasrin Karimi Moayed^{a,*}, Dimitri A.G. Vandenberghe^a, Arne Verbrugge^b,
Souad Ech-Chakrouni^c, Wim De Clercq^d, Johan De Grave^a

^a Laboratory of Mineralogy and Petrology, Department of Geology, Ghent University, Krijgslaan 281 (S8), B-9000, Ghent, Belgium

^b SOLVA, Archaeological Service, Zuid III, Industrielaan 25B, B-9320, Erembodegem, Belgium

^c RMI Geophysical Center at Dourbes, Rue du Centre de Physique 1, B-5670, Viroinval, Dourbes, Belgium

^d Department of Archaeology, Ghent University, Campus UFO, Sint-Pietersnieuwstraat 35, B-9000, Ghent, Belgium

ARTICLE INFO

Keywords:
OSL dating
Hearth
Accuracy
Precision
Modern era

ABSTRACT

Archaeological excavations at “Doorn Noord” (Ninove, East Flanders, Belgium) revealed a complex of traces of human activity and occupation, spanning several millennia. The youngest finds consist of a vast number of surficial hearths and hearth pits, that are interpreted as the remnants of military camps. Based on direct and indirect historical information, as well as a few diagnostic finds, these traces were originally assigned to possible phases of encampment in 1692 CE, 1693 CE, 1745 CE and/or 1831–1838 CE. Although widely used in archaeological research, it is well-known that radiocarbon (¹⁴C) dating lacks precision for post-1650 CE features and therefore does not allow allocating a particular trace to a distinct phase of military presence.

In this study, we report on the potential of optically stimulated luminescence (OSL) signals of quartz for directly dating the heated sedimentary remains of the hearths. We consider it a test of both accuracy and precision given the availability of independent age information (historical sources and archaeomagnetic dating). Six samples from three features yielded indistinguishable optical ages, with an average age of 1748 ± 39 CE (95% probability). This OSL date coincides with historical and archaeological evidence for the presence of a large army in this area in 1745 CE. As sources of systematic uncertainty are (largely) shared, it is possible to distinguish between comparable features with a relative time-resolution of ~2%. For hearths from the last few centuries (post-1650 CE), this implies that numerical and relative chronologies can be established on decadal and multi-annual timescales with 95% confidence.

1. Introduction

The origins of luminescence dating lie in its application to heated materials and objects such as pottery, bricks, tiles, kilns and burnt stones (see e.g. Aitken, 1985; Wagner, 1998). The early work used thermoluminescence (TL) signals. The applications for dating, however, were hampered by poor precision and hence the focus shifted towards authenticity testing for which it is still widely used (e.g. Stoneham, 1991; Leung et al., 2005; Guidorzi et al., 2021). Use of signals stimulated by light (optically stimulated luminescence; OSL), which can also be reset by heat (e.g. Wintle and Murray, 1997), in combination with single-aliquot protocols for measuring dose, offered improved precision (e.g. Liritzis et al., 1994, 1997; Mejdahl and Bøtter-Jensen 1994, 1997; Murray and Mejdahl, 1999; Murray and Wintle, 2000). Such approaches

have been applied to ceramics (or pottery), bricks, burnt sediments and stones, hearths and slags (e.g. Feathers, 2003; Bailiff, 2007; Duller, 2008; Rhodes et al., 2010; Armitage and King, 2013; Yu et al., 2016; Sun et al., 2012, 2018; Wang et al., 2022a, b). While encouraging results have been obtained, a critical review of the literature illustrates that the true potential of OSL-dating of anthropogenically heated materials has remained largely untapped. Indeed, in comparison to OSL-dating of unheated sediments, the available studies on heated materials are limited both in number of publications (see e.g. Bailiff, 2019) and in the types and ages of features investigated. At least to our knowledge, the approach has never before been tested for dating cooking hearths, only in a few studies for directly dating hearths in general (Rhodes et al., 2009, 2010; Armitage and King, 2013; Yu et al., 2016; Sun et al., 2012, 2018), and rarely for tackling chronometric issues that pertain to heated

* Corresponding author.

E-mail address: Nasrin.karimimoayed@ugent.be (N. Karimi Moayed).

materials that date from modern to contemporary times and/or require a decadal time-resolution. One notable exception with respect to the latter concerns the work by [Bailiff \(2007\)](#) on bricks from late-medieval and post-medieval buildings in England. In this paper, we investigate the potential of quartz-based OSL dating for application in this apparently largely un(der)explored area of luminescence chronometric research.

The features studied here are three fireplaces/hearths from (early) modern times that were found during archaeological excavations prior to the construction of a new business park “Doorn Noord” in Ninove (Belgium; [Fig. 1](#)). Excavations over an area of 9 ha ([Fig. 1b](#), light orange area) of the project area of 23 ha ([Fig. 1b](#), red line) in fact revealed approximately 500 of such features, essentially consisting of hearth pits and underground shelters with well-preserved fireplaces or hearths ([Fig. S1](#)). Associated finds include shards of cooking pots, smoker’s pipes, and food waste. As different “types” of pits could be recognized during the excavation, the hypothesis emerged that these traces could point to successive and distinct phases of military encampment. Chronologically diagnostic finds (coins, ceramics, stamped pipes, etc.) are scarce but point at several possible distinct phases, as also suggested by historical sources: 1692 CE, 1693 CE, 1745 CE and 1831–1838 CE. While it is not uncommon to find remains of successive military camps at one particular locality, the large scale of the excavations at “Doorn Noord” is at least regionally unique and may provide specific insights into the history of the armed conflicts in the former Southern Netherlands. However, both the (few) finds associated with the hearths and the historical records provide indirect dating evidence, implying that the vast majority of traces cannot be allocated to a specific period of encampment. This lack of precise and direct time information hampers interpreting a potentially highly detailed record of confrontations in the Low Lands during the 17th to 19th century CE.

Radiocarbon (^{14}C) dating is commonly used to resolve chronological questions in archaeological research but is known to be of limited use for post-1650 CE features ([Stuiver, 1961](#); [Tans et al., 1979](#); [Karimi Moayed et al., 2020](#); [Deforce et al., 2021](#)). It was therefore not considered in the archaeological study of the military camps at Ninove “Doorn Noord”, requiring that alternative chronometric tools are put to use. Archaeomagnetic dating is one such potentially powerful tool, in particular for fired materials, and it can be more precise for those periods where

^{14}C -dating is problematic (e.g. [Linford, 2006](#); [Batt et al., 2017](#)). It was applied to two of the fireplaces/hearths investigated in this paper. The approach requires a calibration curve, however, which is regionally specific and is constructed through archaeomagnetic analysis of known age features. Hence, it would seem desirable to complement – where possible – archaeomagnetic dating by other independent methods. Given the specific possibilities and limitations of each technique, a multi-dating approach is advantageous.

Given that some age information is available through the archaeological finds, historical documents and archaeomagnetic dating, one could consider our OSL-study a test of accuracy and precision in applications that use anthropogenically heated materials. If successful, the results could contribute to an improved understanding of the early-modern and modern features as preserved at Ninove “Doorn Noord”, but also highlight the feasibility of applying OSL as dating tool in relatively recent historical contexts.

2. Material and methods

2.1. Study area and setting

The site “Doorn Noord” is located in the city of Ninove (East-Flanders, Belgium; [Fig. 1a](#)) and extends over an elevated plateau alongside the Dender Valley ([Fig. 1a](#)). It is situated in the Belgian loess belt ([Gullentops et al., 2001](#); [Louis, 1962](#)). The Quaternary cover in the area has been described as consisting of windblown sediments that were deposited during the Weichselian (or perhaps the Early-Holocene) and/or slope deposits ([Fig. 2](#); [Gullentops et al., 2001](#)).

The archaeological research at “Doorn Noord” preceded construction works for a large business park and related roadworks. In the period 2018–2021, an area of 9 ha was excavated. Apart from Final Neolithic burial mounds and the remains of a small Roman settlement, the finds consist of 406 surficial hearths and hearth pits, as well as pits with hearth niches, spread over an area of over 6.8 ha ([Fig. 1b](#)). Related to these hearths and pits are finds such as ceramics, coins, pipes, glass, flints, spindle whorls, buckles, buttons, glass and musket balls. As the excavation proceeded, and finds were processed and results combined with information gathered from historical cartographic sources, it

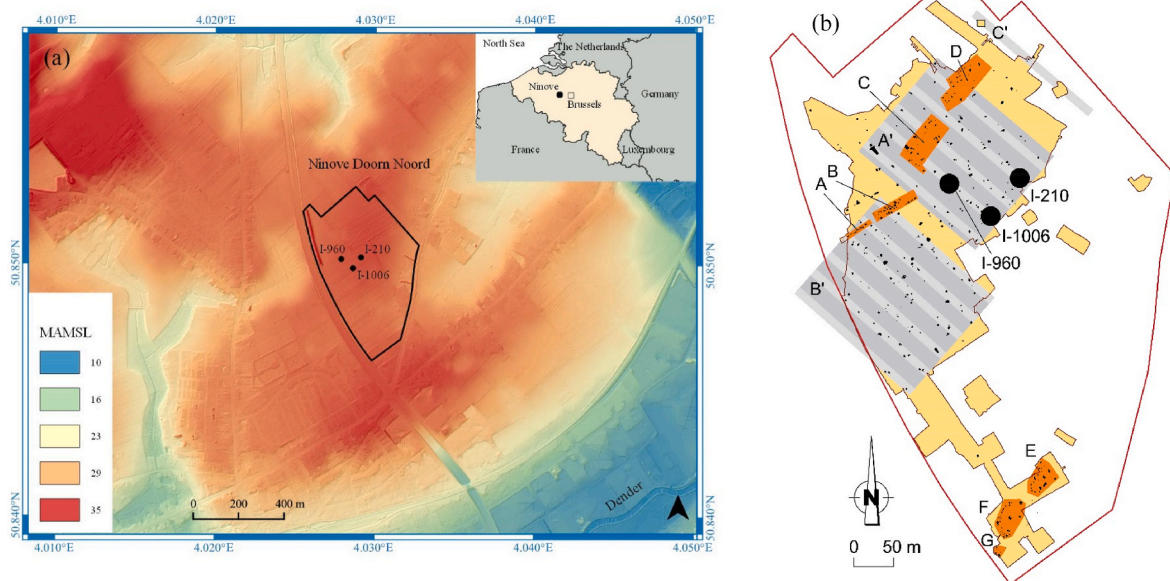


Fig. 1. (a) Digital elevation map showing the project area in “Doorn Noord” in Ninove (black line). The investigated features (I-210, I-960, and I-1006) are indicated by the solid black. MAMSL: Metres Above Mean Sea Level. The inset shows the location of Ninove in Belgium. (b) The red line delimitates the project area (~23 ha); the excavated area (ca. 9 ha) is shaded in light orange. Based on post-excavation reconstruction, the concentrations of traces from the encampment in 1692–1693 CE are indicated by the dark orange blocks (A–G); those from the encampment in 1745 CE by the grey blocks (A'–C').

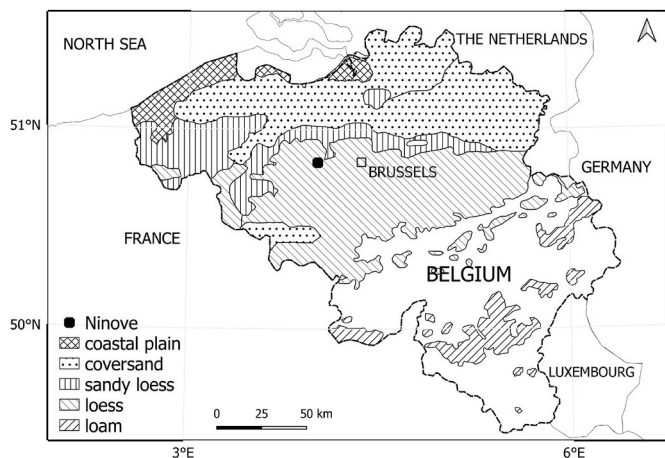


Fig. 2. Schematic map showing the main Quaternary sedimentation areas in Belgium. From <https://ncs.naturalsciences.be/quaternary/introduction-figs>. The location of the study area (Ninove) is indicated by the black solid circle.

became clear that these are the remnants of military camps dating from three possible distinct phases within the early-modern and modern period. The largest structures are interpreted as dug-out shelters, as supported by remains of postholes, stairs, benches, different types of hearth-structures, and chimneys (Fig. S1). The hearth remains in three of these larger structures were selected in the frame of this OSL dating study (Fig. 3a–c; features I-210, I-1006, and I-960); two of these features (I-210 and I-960) were also dated using archaeomagnetism.

2.2. Independent age information

2.2.1. Archaeomagnetic dating

Four hearth-structures were archaeomagnetically dated, of which two (features I-210 and I-960) are directly relevant to this study. Details on the sampling, instrumentation and magnetic measurements are beyond the scope of this paper and were detailed by Souad (2020). The archaeomagnetic dates are based on present knowledge of the secular variation of the field direction during the last three millennia in Western Europe. As the sampling site is located relatively close (~300 km) to the reference site Paris, the directional results were compared with the master secular variation curves of declination and inclination for France (Gallet et al., 2002). The declination and inclination reference curves were obtained using Bayesian hierarchical statistics (Lanos, 2004; Lanos et al., 2005). Following Noël and Batt (1990), probability densities of possible ages were then obtained at the 95% confidence level using the software Rendate (Lanos, 2004; Lanos et al., 2005). Due to the recurrence of the magnetic field, this resulted in multiple time-intervals, with different probabilities. For feature I-960, the archaeomagnetic age ranges are [-324, 77] CE (88.8% probability) and [460, 590] CE (6.2% probability). The age ranges obtained for feature I-210 are [1661, 1825]

CE (67.9% probability) and [-325, -134] CE (27.2% probability). Only the date of [1661–1825] CE is consistent with an early-modern and modern firing event.

2.2.2. Historical information

Several historical sources document the presence of multiple military camps at Ninove. Based on the finds and the historical evidence, the oldest two camps date from the time of the Nine Years' War (1688–1697 CE), between the French army of Louis XIV and the forces of an international coalition led by the king of England William III (Wauters and Verbrugge, 2022; Verbrugge et al., 2022). Apart from numerous newspaper articles, diaries and marching orders, a number of cartographic images were found that show military camps at or near the excavated site “Doorn Noord” in 1692 and 1693 CE.

Local archives and newspapers, as well as a range of military documents and diaries, mention the presence of a French army at Ninove in 1745 CE. This presence and military activity can be associated with the War of the Austrian Succession (1740–1748 CE), in which France, Prussia, and Spain (amongst others) fought against the Austrian empress Maria Theresa and her allies. Although originally fought on Central and Eastern European battlefields, the battleground extended towards the Southern Netherlands from early 1744 CE onwards. Between 8 September and 15 October 1745 CE, the French army settled in Ninove. The 1745-French campaign is well documented, and several written sources locate the camp at Ninove at or near the excavated area.

At the beginning of the excavation and the time of sampling, it was thought that a more recent phase of military encampment dating from 1831 to 1838 CE, might have been preserved as well. This was tentatively deduced from the find of a single copper coin, depicting Leopold I (the first King of Belgium, reigning from 1831 to 1865 CE) and a partially preserved date (“18?8”, with “?” referring to the illegible digit). Post-excavation analysis, however, revealed that only the phases 1692 CE, 1693 CE and 1745 CE are present at Ninove.

2.3. OSL-dating

The remains of three hearths/ovens were selected for OSL dating (features I-210, I-960 and I-1006; Fig. 3a–c). Of interest here are heated sediments that make up the walls and/or base of the hearth pits and alcoves that were dug into the loamy subsurface (Fig. 3 and S1–S3). These structures are well-preserved, although their texture is generally more friable compared to brick. We targeted sediments with clear signs of heating, as suggested by the reddish brick-like colour that is typical for burnt loess; the parent material is yellowish-grey in colour (Figs. S2 and S3). Eight heated sediment samples in total were taken for luminescence analyses (Table 1) using either stainless steel (5 cm diameter; 5 cm long) or opaque PVC tubes (3 cm diameter; 15 cm long). In addition, one sample was taken from sediments that were located close to, but not visibly affected by heating (feature I-960; inset to Fig. 3c; sample GLL-192809 in Table 1). The sediment immediately surrounding each OSL-tube was collected for radionuclide analysis. Two samples were

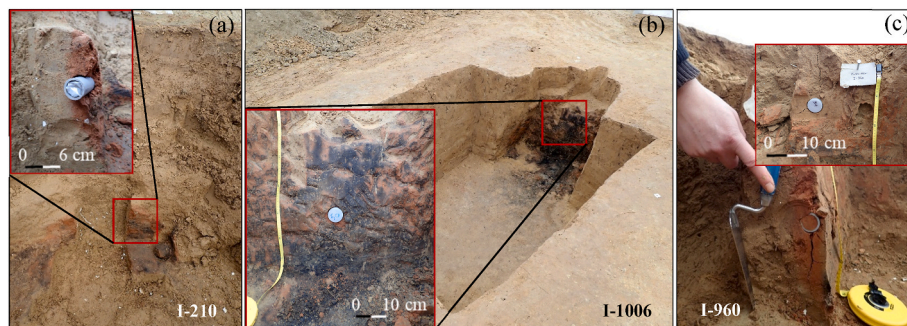


Fig. 3. Photographs illustrating the sampling of features I-210 (a), I-1006 (b) and I-960 (c).

Table 1

Radionuclide activities used for dose-rate evaluation, estimates of time-averaged moisture content ($F \times W$, with the F the fraction of saturation corresponding to the time-averaged moisture content, and W the saturation content as measured in the laboratory), calculated dose rates, equivalent doses (D_e), calculated OSL ages, and random (σ_r), systematic (σ_s) and total uncertainties (σ_{tot}). The OSL ages (± 2 sigma total uncertainties; i.e. random + systematic) are expressed as ages Common Era (CE) in the last column. The burial depth for all samples was estimated at 200 cm.

Feature	Lab code	Material	²³⁴ Th	²²⁶ Ra	²¹⁰ Pb	²³² Th	⁴⁰ K	F × W	Total dose rate	D_e	OSL Age	σ_r	σ_s	σ_{tot}	OSL Age
			(Bq kg ⁻¹)		(Gy ka ⁻¹)	(Gy)	(ka ± 1σ)	(%)	(%)	(%)	(CE ± 2σ)				
I960	192807	Burnt	35 ± 3	42 ± 1	39 ± 2	42 ± 0.5	484 ± 2	0.14 ± 0.04	2.76 ± 0.03	0.769 ± 0.004 ₍₅₂₎	0.28 ± 0.02	1.06	7.23	7.31	1740 ± 41
	192808-X13	Burnt	32 ± 3	42 ± 1	34 ± 5	42 ± 0.4	495 ± 4	0.14 ± 0.04	2.71 ± 0.07	3.0 ± 0.2 ₍₅₁₎	1.09 ± 0.12	7.79	7.24	10.63	925 ± 233
	192809	Unburnt	30 ± 4	42 ± 1	37 ± 3	42 ± 0.5	512 ± 4	0.22 ± 0.02	2.59 ± 0.04	39.6 ± 1.6 ₍₂₇₎	15.3 ± 1.1	4.44	5.92	7.40	-13253 ± 2261
I1006	192811-X13	Burnt	30 ± 2	43 ± 1	33 ± 2	44 ± 0.4	502 ± 5	0.14 ± 0.04	2.75 ± 0.03	0.73 ± 0.01 ₍₅₀₎	0.26 ± 0.02	1.75	7.23	7.44	1754 ± 39
	192812-X14	Burnt	30 ± 2	43 ± 1	33 ± 2	44 ± 0.4	502 ± 5	0.14 ± 0.04	2.75 ± 0.03	0.73 ± 0.02 ₍₅₁₎	0.27 ± 0.02	2.86	7.23	7.78	1752 ± 42
	192813-X14	Burnt	30 ± 2	45 ± 1	35 ± 3	45 ± 0.6	490 ± 4	0.14 ± 0.04	2.76 ± 0.04	0.72 ± 0.01 ₍₅₁₎	0.26 ± 0.02	1.97	7.23	7.49	1759 ± 39
	192815	Burnt	30 ± 2	45 ± 1	35 ± 3	45 ± 0.6	490 ± 4	0.14 ± 0.04	2.76 ± 0.04	0.98 ± 0.04 ₍₄₆₎	0.35 ± 0.03	4.61	7.23	8.57	1664 ± 61
I210	192816-X13	Burnt	39 ± 2	41 ± 1	55 ± 3	41 ± 0.4	501 ± 4	0.14 ± 0.04	3.02 ± 0.04	0.797 ± 0.004 ₍₄₈₎	0.26 ± 0.02	1.47	7.25	7.39	1755 ± 39
	192817	Burnt	30 ± 4	40 ± 1	41 ± 2	39 ± 0.6	477 ± 4	0.14 ± 0.04	2.71 ± 0.03	0.79 ± 0.01 ₍₄₀₎	0.29 ± 0.02	1.50	7.22	7.37	1728 ± 43

collected for determining the water content at saturation; the average of these two samples was used in the calculations.

While we aimed at sampling only the sediments that were most likely sufficiently heated, it could not be excluded that some of the sampling tubes penetrated parent material. In addition, any thermal gradient could result in homogeneous incomplete resetting. For most of the samples, we therefore extracted the inner material of the tubes in intervals of approximately 1 cm (Fig. S3). Quartz grains from the 63–250 μm fraction were then isolated following widely adopted procedures (HCl, H₂O₂, sieving, HF; e.g. Murray et al., 2021). For luminescence measurements, quartz grains were spread out on the inner 2 mm (small aliquots) of stainless-steel discs with a thickness of 0.5 mm and a diameter of 9.7 mm, using silicon spray as adhesive. The measurements were carried out using an automated Risø TL/OSL reader equipped with blue ($\lambda_{max} = 470$ nm) and infrared ($\lambda_{max} = 850$ nm) light emitting diodes estimated to deliver about 32 mW/cm² and 108 mW/cm² at the sample position, respectively (Sørensen P., Risø DTU, priv. Comm., 2023). The optically stimulated luminescence signals were detected through 7.5 mm of Hoya U-340 UV filter; irradiations were performed using a calibrated ⁹⁰Sr/⁹⁰Y beta-source mounted on the reader. Details on the facilities can be found in Botter-Jensen et al. (2003, 2010) and Lapp et al. (2015). The luminescence characteristics and equivalent doses (D_e) were determined using the single-aliquot regenerative-dose (SAR) protocol (Murray and Wintle, 2000, 2003). Unless stated otherwise, a preheat at 180 °C for 10 s and a cut heat to 160 °C were adopted. Optical stimulation was for 38.5 s at 125 °C. All the measurements used the first 0.31 s of the decay curve minus a background derived from the following 0.77 s (“early-background subtraction”; Cunningham and Wallinga, 2010). Each measurement of the response to the test dose (2 Gy) was followed by a stimulation for 38.5 s with the blue diodes at 280 °C to minimize recuperation (Murray and Wintle, 2003). For each aliquot, the sensitivity to stimulation with infrared light was measured (OSL IR depletion ratio; Duller, 2003), to check for the presence of feldspar. The sensitivity to infrared stimulation was defined as significant if this ratio deviated more than 10% from unity; no aliquots had to be rejected on this basis. Where applicable, the luminescence analyses focused on the samples from those intervals which, following an initial screening, showed the lowest estimates of D_e and were therefore expected to have been sufficiently heated during the last firing event (Fig. S3 and Table S1). The

sediment collected for dose rate determination was dried at 110 °C (until constant weight), pulverized and homogenized. A subsample (~140 g) of the powdered sediment was then cast in wax (De Corte et al., 2006) and stored for at least one month before being measured on top a low-level extended energy-range HPGe gamma-ray spectrometer. The specific activities were converted to dose rates using conversion factors calculated from the nuclear data tabulated by Adamiec and Aitken (1998). A beta attenuation factor of 0.90 ($\pm 5\%$ relative uncertainty) was adopted to correct the external beta dose rates for the effects of attenuation and etching (Mejdahl, 1979). Correction for the effect of moisture was performed as outlined in Aitken (1985). The subsurface of the study area has been described as consisting of dry loess (Louis, 1962). For the heated sediment samples, we therefore assumed that the time-averaged moisture content during burial equals half the value at saturation; a relative uncertainty of $\pm 30\%$ (1 sigma) was associated with this estimate. For the sample collected from the unheated sediments (GLL-192809), we followed Aitken (1985) and assumed an average water content corresponding to 80% of saturation (with a relative uncertainty of $\pm 8\%$, 1 sigma). An internal dose rate in quartz grains of 0.013 ± 0.003 Gy ka⁻¹ was adopted (Vandenberghe et al., 2008). The contribution of cosmic rays was calculated following Prescott and Hutton (1994), and a 15% relative uncertainty was associated with the values.

3. Results

3.1. Luminescence characteristics and procedural tests

Fig. 4a shows the natural and regenerated OSL decay curve for an aliquot of sample GLL-192807. The signals are clearly distinguishable from the background level and decay rapidly with stimulation time. The decay matches that observed for calibration quartz (Fig. 4a, inset), as expected for a signal dominated by the fast component. The growth of the OSL signal as a function of dose can be well approximated by a single saturating exponential function (solid black line in Fig. 4b). The dose response passes through the origin, indicating that recuperation is negligible (open square). It is possible to reproduce a regenerated dose point implying that sensitivity changes are accurately corrected for (the solid and open circles are overlying each other, i.e. a recycling ratio

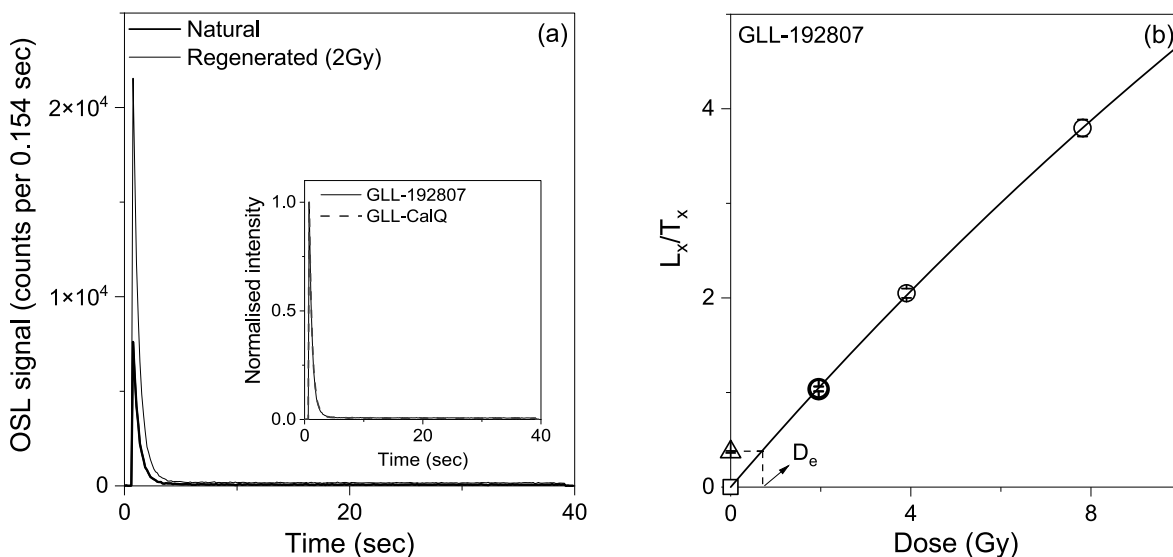


Fig. 4. (a) OSL decay curves for a single aliquot of quartz grains extracted from sample GLL-192807. The natural and regenerated signals are shown as the black and grey lines, respectively. The inset compares the regenerated OSL decay curve from the sample with that from calibration quartz (GLL-CalQ). (b) SAR growth curve for a single aliquot of the same sample. Recycling and recuperation points are represented by the open circle and square, respectively. The solid line is the fit of the data to a single saturating exponential function. The equivalent dose (D_e) is obtained by interpolating the natural sensitivity-corrected OSL signal (open triangle) on the SAR dose response curve.

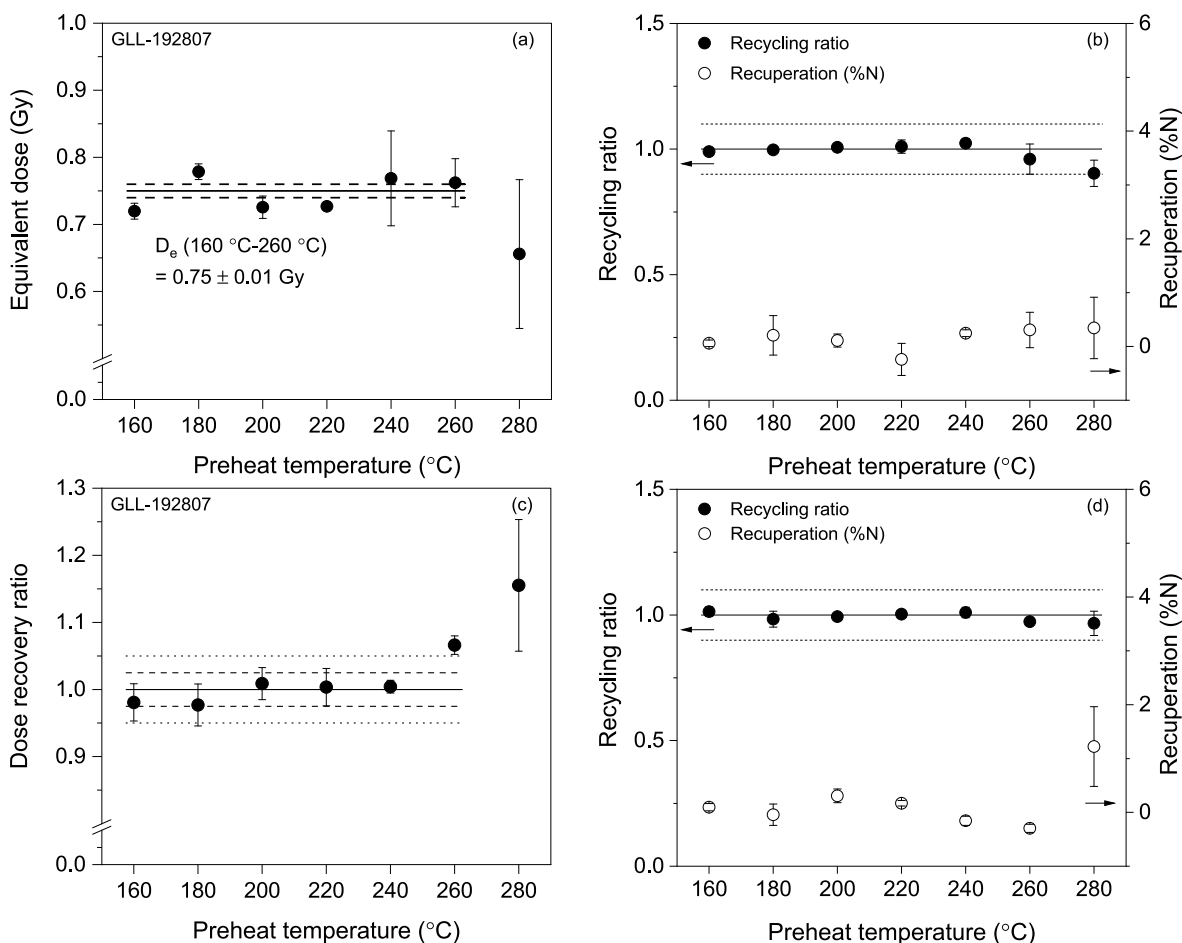


Fig. 5. (a) Dependence of equivalent dose (D_e) on preheat temperature for sample GLL-192807. The dashed and dotted lines indicate the average ± 1 standard error over the 160 °C–260 °C temperature interval. (b) Corresponding recycling and recuperation data; the solid and dashed lines (eye guides) bracket a value for the recycling ratio of 1.0 ± 0.1 . (c) Dependence of dose recovery ratio on preheat temperature for sample GLL-192807. Each data point represents the average (± 1 standard error) of 5 measurements. The dashed and dotted lines are eye guides and bracket a 2.5% and 5% deviation of the ratio from unity (solid line). (d) Corresponding recycling and recuperation data; the solid and dashed lines (eye guides) bracket a value for the recycling ratio of 1.0 ± 0.1 .

equal to unity). For the sake of comparison, the OSL decay and dose response curves from an aliquot of the unheated sample GLL-192809 are shown in Fig. S4. This sample exhibits a significantly lower luminescence sensitivity, indicating that the other samples were indeed sensitized through heating.

To identify the optimum measurement parameters for D_e determination, we examined the dependence of measured dose on preheat temperature using sample GLL-192807. In a first test, groups of three natural aliquots were measured at each of seven different preheat temperatures in the range of 160 °C–280 °C. There is no dependence of D_e on preheat temperature up to 260 °C (Fig. 5a); across this interval, recycling ratios are consistent with unity and recuperation is less than 1% of the sensitivity-corrected natural OSL signal (Fig. 5b). In a second test, natural aliquots were first exposed twice to the blue diodes for 250 s at room temperature, with a 10,000 s pause in between. The aliquots were then given a dose close to the expected natural dose, and measured at each of seven different preheat temperatures in the range of 160 °C–280 °C. The results are shown in Fig. 5c. Across the 160 °C–240 °C temperature interval, the measured doses are consistent with the known given dose; the recycling ratios are consistent with unity as well, and recuperation remains below 1% of the corrected natural OSL signal (Fig. 5d). This second test is known as a dose recovery test and is the most complete test for assessing the performance of a particular SAR procedure for a sample (e.g. Murray et al., 2021). The dose recovery test was repeated, this time using 6 natural aliquots for each of the eight heated sediment samples, and a preheat of 10 s at 180 °C only. The results are summarised in Fig. 6. For all samples except GLL-192811, and within 1 standard error, the measured dose does not differ from the known given dose by more than 2.5% (Fig. 6a). The discrepant result for sample -11, with an unweighted average dose recovery ratio (± 1 standard error) of 0.81 ± 0.14 , is not understood. It results essentially from a very poor and significantly less precise dose recovery value ($\sim 50\%$ relative uncertainty) for one out of the six aliquots measured. Rejecting this aliquot from the analyses yields an average dose recovery

ratio for this sample of 0.92 ± 0.09 . Apart from poor precision, however, there is no other argument (e.g. on the basis of recycling or OSL IR depletion ratio, or recuperation) for rejecting this aliquot. The overall dose recovery ratio (± 1 standard error; $n = 48$) is 0.98 ± 0.03 (Fig. 6b). Taking this as an average descriptor (Murray et al., 2021) suggests that the chosen experimental SAR parameters can accurately measure a known laboratory dose.

3.2. Equivalent dose determination

The equivalent dose in all samples was determined using the SAR protocol, as outlined in the above and using a preheat of 10 s at 180 °C. In between 48 and 52 small aliquots were measured for each burnt sample. All aliquots emitted a net natural test dose signal (“ T_n ”) higher than three times the standard deviation of the background signal and were therefore included in the analyses. The results are shown as histograms in Fig. 7 for two samples of each heated feature and in Fig. S5 for the rest samples in this study.

Except for samples GLL-192808-X13 (feature I-960; Fig. 7b) and -15 (feature I-1006; Fig. S5c) the datasets mainly consist of values that appear to belong to a single dose population and a few aliquots that yielded significantly higher D_e 's. For all measured aliquots, the recycling ratios are close to one and the recuperation is negligible. D_e values that differed by more than three standard deviations from the mean were iteratively rejected and the unweighted mean (± 1 standard error) of the resulting distribution was used in the calculations (Table 1). The unburnt sample GLL-192809 yielded a significantly higher D_e (~ 40 Gy) as would be expected for parent material that was not or only partially heated (Table 1; Fig. S5a).

3.3. OSL ages

Table 1 summarises the analytical data, the calculated dose rates and optical ages. Uncertainties on the OSL ages were calculated following

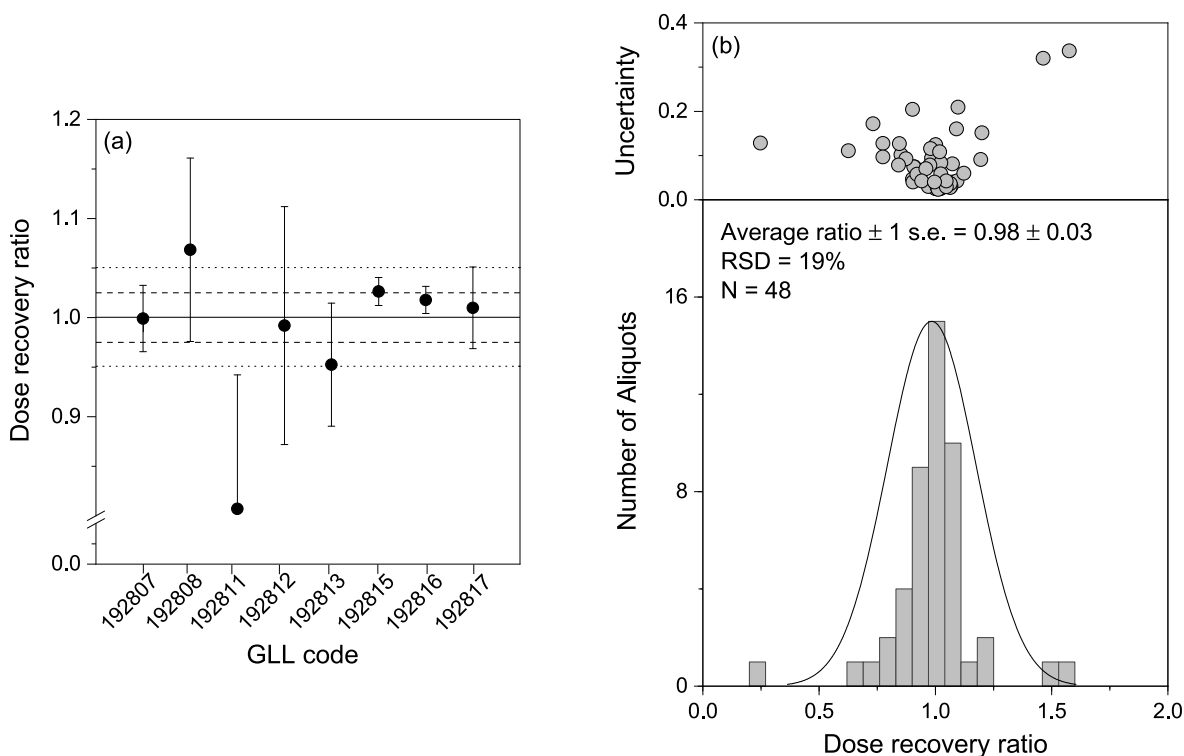


Fig. 6. (a) Average dose recovery ratios (± 1 standard error) obtained for each sample using a preheat of 10 s at 180 °C and a cut heat to 160 °C. The dashed and dotted lines (eye guides) bracket a 2.5% and 5% deviation of the ratio from unity (solid line). (b) Summary of dose recovery data for all samples and aliquots, represented as a histogram.

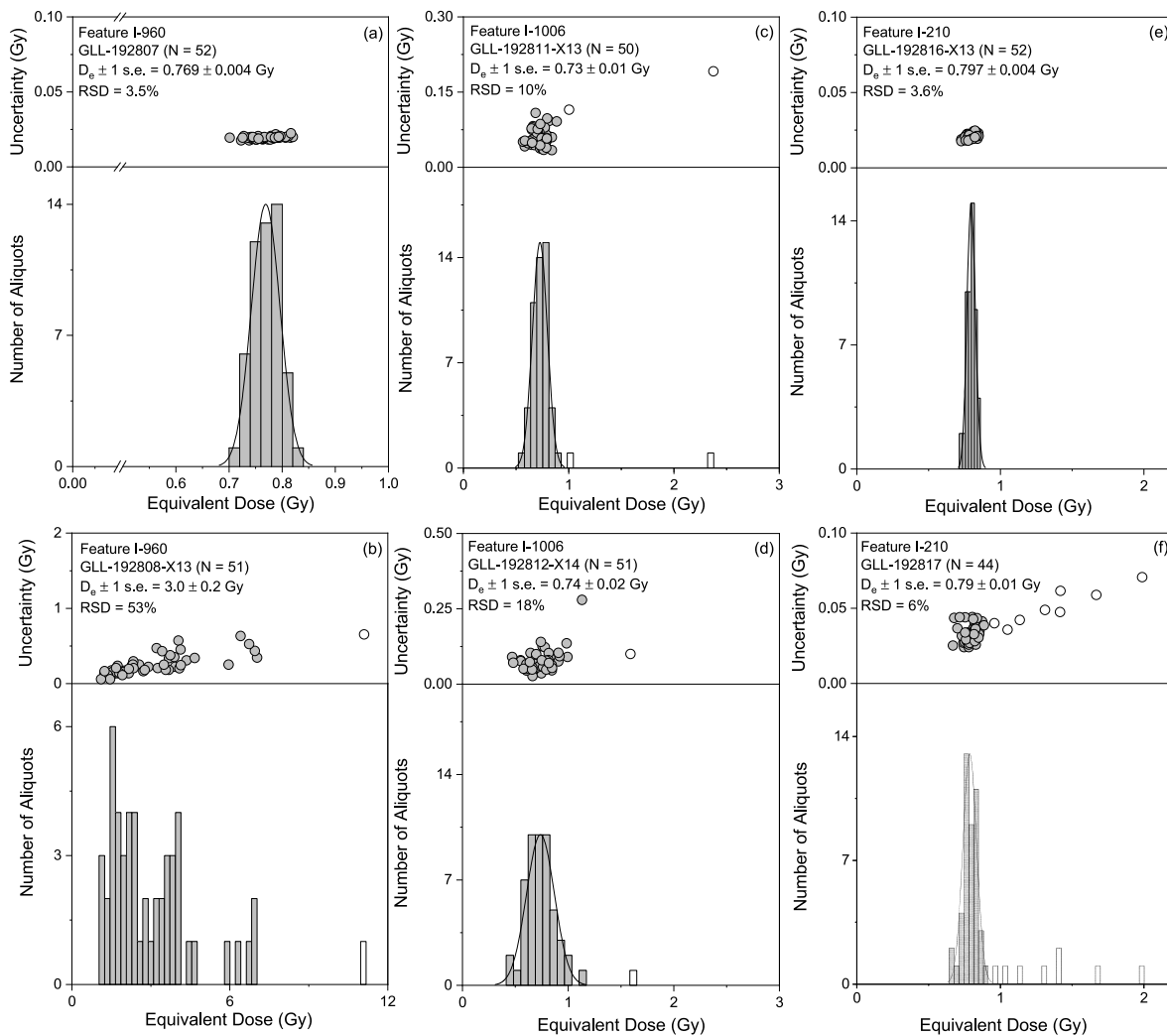


Fig. 7. Distribution of equivalent dose in small (2 mm diameter) aliquots of two samples from each of the three investigated features. (a–b) I-960, samples GLL-192807 & –08; (c–d) I-1006, samples GLL-192811 & –12; (e–f) I-210: samples GLL-192816 & –17.

the error assessment system formalised by Aitken (1985). Additional information on the different sources of systematic uncertainty and their quantification can be found in Vandenberghe et al. (2004). The total uncertainty on the optical ages for the burnt samples ranges between ~7 and 11%; systematic sources of uncertainty are the main contributor. Excluding sample GLL-192808-X13 (owing to the large spread in D_e with an RSD of 53% after excluding the outlier; Fig. 7b), the relative total random uncertainties remain below 5%, and can be as low as ~1–3%. If one assumes that the uncertainties resulting from systematic effects are largely shared between the samples – an assumption that might hold to a certain extent for the different samples from the three heated features at this locality – only the random uncertainties are relevant for intercomparison of the optical ages.

Sample GLL-192815 yields an optical age of 0.35 ± 0.02 ka (1 sigma random uncertainty), with a somewhat higher and more asymmetric spread in D_e compared to the other three samples for the same feature (I-1006; see Fig. 7c–d and Figs. S2b–c); the latter yield a younger and internally consistent set of ages in between 0.260 ± 0.005 ka and 0.267 ± 0.008 ka (1 sigma random uncertainty; Table 1). The two samples taken from feature I-210 yield ages (± 1 sigma random uncertainty) of 0.264 ± 0.004 ka and 0.291 ± 0.004 ka. These ages are not consistent within 2 sigma. Based on our analysis of the D_e -distributions (Fig. 7e–f) there is no particular reason why the average D_e in one of these samples would be less, or more, reliable than the other. An optical age of 0.279 ± 0.003 ka was obtained for sample GLL-192807 (feature I-960; for the

reason outlined in the above, sample –08-X13 is excluded). Based on the distributions of D_e in samples GLL-192808 and –15, we interpret the ages for these two samples as most likely not accurately recording the last heating event.

Taking everything together and considering that the random uncertainty represents a minimum for the limit on precision, we consider six samples (GLL-192807, –11, –12, –13, –16 and –17), and hence the three investigated features, to be coeval. Their average age ($n = 6$; ± 1 sigma total uncertainty; calculated following Aitken, 1985) is 0.271 ± 0.020 ka, or 1748 ± 20 CE.

Sample GLL-192809, which was taken from sediments that were not visibly affected by heating, yields an optical age of 15.3 ± 1.1 ka.

4. Discussion

Fig. 8 compares the archaeomagnetic and historical age information (section 2.2) with the eight OSL ages obtained for the heated sediment samples from the investigated features (section 3.3). Archaeomagnetic and OSL data are compared within 95% probability (2 sigma). Unless stated otherwise, the uncertainties on the OSL ages refer to the 2 sigma total uncertainties (i.e. derived from the combined random and systematic sources of uncertainty).

For feature I-960, the archaeomagnetic age as well as the OSL age for sample GLL-192808 significantly overestimate any possible date for military encampment during the early-modern and modern period. OSL-

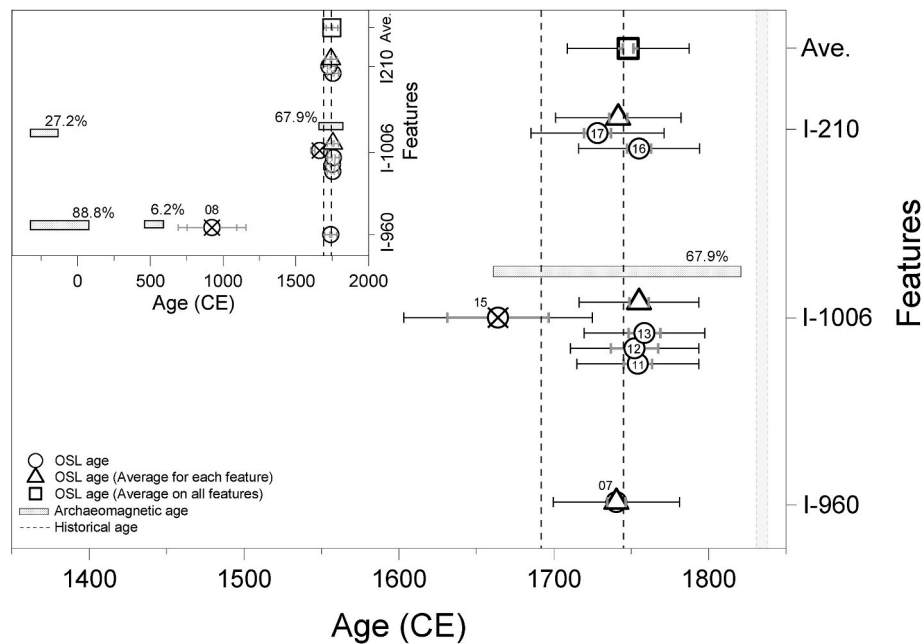


Fig. 8. Comparison between OSL ages, archaeomagnetic age probability distributions, and historical age information. The uncertainties on the OSL and archaeomagnetic ages cover 95.4% probability (2 sigma). Open circles represent the OSL age obtained for each sample, with the two that are crossed out referring to those that were not considered in the discussion (see sections 3.3 and 4 for details). The open triangles indicate the average OSL age for each feature; the open square shows the overall average OSL age. The random and total uncertainties on the OSL ages are indicated by the grey and black error bars, respectively. The archaeomagnetic age probabilities are indicated by the horizontal bars. The vertical dashed lines represent the possible phases of military encampment as derived from historical sources (1692–1693 CE and 1745 CE).

sample -08 was not expected to yield an accurate age, based on the distribution of D_e (Fig. 7b). The OSL age of 1740 ± 41 CE for sample -07 matches historical evidence for encampment in the middle 18th century (1745 CE).

An archaeomagnetic date is also available for feature I-1006; the age interval of [1661, 1825] CE (67.9% probability) is consistent with the OSL-ages for samples -11, -12 and -13. The average OSL age for these three samples is 1755 ± 39 CE and would allocate this feature to the 1745 CE encampment. Sample -15 yields an older date of 1664 ± 61 CE, which is not inconsistent with historical evidence (1692–1693 CE or 1745 CE). In comparison to the other samples, however, the D_e 's are spread over a larger range. While this spread could be sample intrinsic, the age result is not internally consistent with the three other OSL-dates for this same feature. Two OSL ages were obtained for feature I-210, which would allocate the hearth to either 1692–1693 CE, or 1745 CE. The OSL ages are not entirely internally consistent, and our experimental data do not allow identifying why one date should be preferred over the other (section 3.3). The average OSL age dates this feature to 1742 ± 41 CE.

None of the OSL age results for the three investigated features provides evidence for them to be linked to a military encampment during 1831–1838 CE, which matches the insights gained from post-excavational analyses (section 2.2.2). In the following discussion, we exclude the OSL-results obtained for samples GLL-192808 and -15, for the reasons outlined higher.

Within two sigma total uncertainties, all dates are clearly centred around 1745 CE (Fig. 8), suggesting that the samples and hearths are coeval. Averaging the results for these six samples yields a date of 1748 ± 39 CE. The uncertainty essentially arises from systematic effects, such as that associated with our estimate of past water content. Increasing the time-averaged water content with 1%, increases the optical age by about 1%. Given that no factual information is available on past water content, we adopted half of the value at saturation with an uncertainty that covers all plausible scenarios within 3 sigma (i.e. from almost completely dry, to almost saturated). While this is - at least in our

opinion - an objective analysis of uncertainty, it does cover a wide range and might be an overestimate.

The comparison between the archaeomagnetic and OSL dates is of interest. In the present context, both aimed at establishing the time when the sediment was heated to a sufficiently high temperature. They differ, however, in the physical mechanisms that are exploited for dating as well as in the temperatures involved, the way and scale of sampling, subsequent analysis and age calculation. A detailed discussion is beyond the scope of this paper. We limit ourselves here to how OSL might potentially provide information for archaeomagnetic dating. Firstly, the D_e -distributions in sample GLL-192808 (feature I-960) and possibly -15 (feature I-1006) indicated that these might be problematic in terms of resetting and/or disturbance. These effects can be expected to affect archaeomagnetic dating, even more so as larger volumes of samples are taken. While our dataset is limited, the results obtained for sample -08 (Fig. 7b) may very well relate to the apparent significant overestimate in the archaeomagnetic age. Secondly, archaeomagnetic dating needs calibration data obtained through archaeomagnetic analysis of features with independent age control, and results in possible age-probability intervals (comparable to ^{14}C). OSL dating does not require calibration in this manner and therefore can contribute to improving archaeomagnetic calibration data bases.

The 1 sigma total uncertainty associated with an individual OSL age is ~ 7–8% (Table 1) and is relevant when comparing the dates with other chronological information. For comparison between the OSL ages amongst each other and given that they were obtained for (very) similar features at the same site/locality, the random uncertainties are relevant. These are in the range of 1–3%. As noted for feature I-210 (samples GLL-192816 and -17) and assuming that both ages are accurate and refer to the same event, however, the observed variability can be higher (~5%). If the dataset is extended to multiple coeval samples from different features - here taken to be samples GLL-192807, -11, -12, -13, -16 and -17, covering the three features - the observed level of precision is ~2%, comparable to the overall expected random uncertainty of ~1%. Within the time range under consideration here, this implies the

possibility of distinguishing between features with a resolution of about 10 years, with 95% probability.

5. Conclusions

An average OSL date (± 2 sigma total uncertainty; six samples) of 1748 ± 39 CE was obtained for three hearth/oven remains at Doorn-Noord, Ninove (Belgium). This OSL date matches historical and archaeological evidence for a French military camp, situated at this locality in 1745 CE, from which we conclude that it is accurate. In turn, it allows allocating these traces directly to this specific phase of encampment.

The OSL dates also match one archaeomagnetic age interval but are considerably more precise. The results illustrate how OSL dating of heated features can help improving the quality of archaeomagnetic intensity calibration data bases, and aid in assessing the suitability of a sample for archaeomagnetic analysis. This is important, as also archaeomagnetic dating offers great potential for the periods where radiocarbon dating is problematic.

In addition, our study reinforces the added value of dating multiple OSL-samples from a single feature, and of doing so for multiple features. We demonstrate that this strategy may allow distinguishing, relatively, between comparable features at decadal timescales, with 95% confidence. At least to our knowledge, this is an exceptional level of precision, which could greatly benefit archaeological studies of this type of remains from last few centuries. Apart from the apparent level of accuracy that can be achieved through OSL-dating, we highlight its possibilities for addressing chronometric issues that require high time-resolution.

In general, we conclude that the OSL-methodology reported upon is not limited to the specific type (cooking hearths) and age range of features investigated here. At least in principle, it is applicable to a wide range of (anthropogenically) heated sediments that can be found all over the world in various contexts. Amongst the most important prerequisites are completeness of resetting of the luminescence clock in the past, suitability of the signal characteristics and accurate assessment of the dose rate. One advantage of OSL-dating over other chronometric methods is that these potentially limiting factors can be experimentally assessed. The precision on the numerical ages obtained can be as good as ~ 7 –8%, and a relative time-resolution of $\sim 2\%$ can be achieved. The latter implies that similar features of about 100 years old can be distinguished to within ~ 2 years, those of about 1000 years old to within 20 years, etc. We consider the approach particularly advantageous for application to heated siliciclastic remnants from relatively recent times (i.e. early modern times and later) for which it is difficult or even impossible to obtain meaningful age information using other chronometric methods.

Declaration of competing interest

The authors declare that they have no known competing financial interests or personal relationships that could have appeared to influence the work reported in this paper.

Acknowledgments

This research was partially funded by the UGent Special Research Fund in the frame of the Interdisciplinary Research Project “Fueling the Furnace. An interdisciplinary study of forest soils as geoarchaeological archives” (BOF-IOP project number 01IO3318). We thank Drs. Krista Frickelo for logistic support. The technical assistance of Ann-Eline Debeer is appreciated. This paper is dedicated to Prof. Dr. Morgan De Dapper in recognition of two decades of fruitful collaboration, support and endeavours in broadening horizons.

Appendix A. Supplementary data

Supplementary data to this article can be found online at <https://doi.org/10.1016/j.jas.2023.105858>.

References

- Adamiec, G., Aitken, M.J., 1998. Dose-rate conversion factors: update. *Ancient TL* 16, 37–50.
- Aitken, M.J., 1985. *Thermoluminescence Dating*, vol. 359p. Academic Press, London, 0-12-046380-6.
- Armitage, S.J., King, G.E., 2013. Optically stimulated luminescence dating of hearths from the Fazzan Basin, Libya: a tool for determining the timing and pattern of Holocene occupation of the Sahara. *Quat. Geochronol.* 15, 88–97. <https://doi.org/10.1016/j.quageo.2012.10.002>.
- Batt, C.M., Brown, M.C., Clelland, S.J., Korte, M., Linford, P., Outram, Z., 2017. Advances in archaeomagnetic dating in Britain: new data, new approaches and a new calibration curve. *J. Archaeol. Sci.* 85, 66–82. <https://doi.org/10.1016/j.jas.2017.07.002>.
- Bailliff, I.K., 2007. Methodological developments in the luminescence dating of brick from English Late-Medieval and Post-Medieval buildings. *Archaeometry* 49, 827–851. <https://doi.org/10.1111/j.1475-4754.2007.00338.x>.
- Bailliff, I.K., 2019. Applications in archaeological contexts. In: Bateman, M. (Ed.), *Handbook of Luminescence Dating*. Whittles Publishing, Dunbeath, pp. 321–349.
- Bøtter-Jensen, L., Andersen, C.E., Duller, G.A.T., Murray, A.S., 2003. Developments in radiation, stimulation and observation facilities in luminescence measurements. *Radiat. Meas.* 37, 535–541. [https://doi.org/10.1016/S1350-4487\(03\)00020-9](https://doi.org/10.1016/S1350-4487(03)00020-9).
- Bøtter-Jensen, L., Thomsen, K.J., Jain, M., 2010. Review of optically stimulated luminescence (OSL) instrumental developments for retrospective dosimetry. *Radiat. Meas.* 45, 253–257. <https://doi.org/10.1016/j.radmeas.2009.11.030>.
- Cunningham, A.C., Wallinga, J., 2010. Selection of integration time intervals for quartz OSL decay curves. *Quat. Geochronol.* 5, 657–666.
- De Corte, F., Vandenberghe, D., De Wispelaere, A., Buylaert, J.P., Van den haute, P., 2006. Radon loss from encapsulated sediments in Ge gamma-ray spectrometry for the annual radiation dose determination in luminescence dating. *Czech. J. Phys.* 56, D183–D194. <https://doi.org/10.1007/s10582-006-0504-9>.
- Deforce, K., Groenewoudt, B., Haneca, K., 2021. 2500 years of charcoal production in the Low Countries: the chronology and typology of charcoal kilns and their relation with early iron production. *Quat. Int.* 593–594, 295–305. <https://doi.org/10.1016/j.quaint.2020.10.020>.
- Duller, G.A.T., 2003. Distinguishing quartz and feldspar in single grain luminescence measurements. *Radiat. Meas.* 37, 161–165. [https://doi.org/10.1016/S1350-4487\(02\)00170-1](https://doi.org/10.1016/S1350-4487(02)00170-1).
- Duller, G.A.T., 2008. *Luminescence Dating: Guidelines on Using Luminescence Dating in Archaeology*. English Heritage, Swindon, p. 45pp.
- Feathers, J.K., 2003. Use of luminescence dating in archaeology. *Meas. Sci. Technol.* 14, 1493–1509. <https://doi.org/10.1088/0957-0233/14/9/302>.
- Gallet, Y., Genevey, A., Le Goff, M., 2002. Three millennia of directional variations of the Earth's magnetic field in Western Europe as revealed by archaeological artefacts. *Phys. Earth Planet. In.* 131, 81–89. [https://doi.org/10.1016/S0031-9201\(02\)00030-4](https://doi.org/10.1016/S0031-9201(02)00030-4).
- Guidorzi, L., Fantino, F., Durisi, E., Ferrero, M., Re, A., Vigorelli, L., Visca, L., Gulmini, M., Dughera, G., Giraudo, G., Angelici, D., Panero, E., Giudice, A.L., 2021. Age determination and authentication of ceramics: advancements in the thermoluminescence dating laboratory in Torino (Italy). IMEKO International Measurement Confederation in *Acta Imeko* 10, 32–39. https://doi.org/10.21014/acta_imeko.v10i1.813.
- Gullentops, F., Bogemans, F., De Moor, G., Paulissen, E., Pissart, A., 2001. Quaternary lithostratigraphic units (Belgium). In: Bultynck, P., Dejonghe, L. (Eds.), *Guide to a Revised Lithostratigraphic Scale of Belgium*, *Geologica Belgica* 4/1-2, Bruxelles, pp. 153–164.
- Karimi Moayed, N., Vandenberghe, D.A.G., Deforce, K., Bastiaens, J., Ghyselbrecht, E., Debeer, A.E., De Grave, J., 2020. Bypassing the Suess-effect: age determination of charcoal kiln remains using OSL dating. *J. Archaeol. Sci.*, 105176 <https://doi.org/10.1016/j.jas.2020.105176>.
- Lanos, Ph., 2004. Bayesian inference of calibration curves: application to archaeomagnetism, in tools for constructing chronologies: crossing disciplinary boundaries. *Lect. Notes Stat.* 177, 43–82.
- Lanos, Ph., Le Goff, M., Kovacheva, M., Schnepf, E., 2005. Hierarchical modeling of archaeomagnetic data and curve estimation by moving average technique. *Geophys. J. Int.* 160, 440–476. <https://doi.org/10.1111/j.1365-246X.2005.02490.x>.
- Lapp, T., Kook, M., Murray, A.S., Thomsen, K.J., Buylaert, J.P., Jain, M., 2015. A new luminescence detection and stimulation head for the Risø TL/OSL reader. *Radiat. Meas.* 81, 178–184. <https://doi.org/10.1016/j.radmeas.2015.02.001>.
- Leung, P.L., Tang, Q., Li, M., Zhang, C., 2005. The preliminary application of OSL in comparison with TL for authentication of ancient Chinese bricks. *Radiat. Meas.* 40, 1–4. <https://doi.org/10.1016/j.radmeas.2004.05.012>.
- Linford, P., 2006. *Archaeomagnetic Dating: Guidelines on Producing and Interpreting Archaeomagnetic Dates*. English Heritage, Swindon. <http://dourbes.meteo.be/aarch-net/linford.pdf>.
- Louis, A., 1962. Verklarende tekst bij het kaartblad Ninove 86 E. In: *Bodemkaart Van België*, LWONL. Gent.

- Liritzis, I., Galloway, R.B., Hong, D.G., 1997. Single aliquot dating of ceramics by green light stimulation of luminescence from quartz. *Nucl. Instrum. Methods Phys. Res. B* 132, 457–467. [https://doi.org/10.1016/S0168-583X\(97\)00456-4](https://doi.org/10.1016/S0168-583X(97)00456-4).
- Liritzis, I., Galloway, R.B., Theocrats, T.S., 1994. Thermoluminescence dating of ceramics revisited: optical stimulated luminescence of quartz single aliquot with green light-emitting diodes. *J. Radioanal. Nucl. Chem.* 188, 189–198. Letters.
- Mejdahl, V., 1979. Thermoluminescence dating: beta-dose attenuation in quartz grains. *Archaeometry* 21, 61–72.
- Mejdahl, V., Bøtter-Jensen, L., 1994. Luminescence dating of archaeological materials using a new technique based on single aliquot measurements. *Quat. Geochronol.* 13, 551–554. [https://doi.org/10.1016/0277-3791\(94\)90076-0](https://doi.org/10.1016/0277-3791(94)90076-0).
- Mejdahl, V., Bøtter-Jensen, L., 1997. Experience with the SARA OSL method. *Radiat. Meas.* 27, 291–294. [https://doi.org/10.1016/S1350-4487\(96\)00149-7](https://doi.org/10.1016/S1350-4487(96)00149-7).
- Murray, A.S., Mejdahl, V., 1999. Comparison of regenerative-dose single-aliquot and multiple-aliquot (SARA) protocols using heated quartz from archaeological sites. *Quat. Geochronol.* 18, 223–229. [https://doi.org/10.1016/S0277-3791\(98\)00055-9](https://doi.org/10.1016/S0277-3791(98)00055-9).
- Murray, A.S., Wintle, A.G., 2000. Luminescence dating of quartz using an improved single-aliquot regenerative-dose protocol. *Radiat. Meas.* 32, 57–73. [https://doi.org/10.1016/S1350-4487\(99\)00253-X](https://doi.org/10.1016/S1350-4487(99)00253-X).
- Murray, A.S., Wintle, A.G., 2003. The single aliquot regenerative dose protocol: potential for improvements in reliability. *Radiat. Meas.* 37, 377–381. [https://doi.org/10.1016/S1350-4487\(03\)00053-2](https://doi.org/10.1016/S1350-4487(03)00053-2).
- Murray, A.S., Arnold, L.J., Buylaert, J.P., Guérin, G., Qin, J., Singhvi, A.K., Smedley, R., Thomsen, K.J., 2021. Optically stimulated luminescence dating using quartz. *Nature Reviews, Methods Primers* 1, 72. <https://doi.org/10.1038/s43586-021-00068-5>.
- Noël, M., Batt, C., 1990. A method for correcting geographically separated remanence directions for the purpose of archaeomagnetic dating. *Geophys. J. Int.* 102, 753–756.
- Prescott, J.R., Hutton, J.T., 1994. Cosmic ray contributions to dose rates for luminescence and ESR dating: large depths and long-term time variations. *Radiat. Meas.* 23, 497–500.
- Rhodes, E.J., Fanning, P.C., Holdaway, S.J., Bolton, C.C., 2009. Archaeological surfaces in western NSW: stratigraphic contexts and preliminary OSL dating of hearths. *Terra Aust.* 28, 189–200.
- Rhodes, E.J., Fanning, P.C., Holdaway, S.J., 2010. Developments in optically stimulated luminescence age control for geoarchaeological sediments and hearths in western New South Wales, Australia. *Quat. Geochronol.* 5, 348–352. <https://doi.org/10.1016/j.quageo.2009.04.001>.
- Souad, E.-C., 2020. Archeomagnetische Datering Van Verbarande Structuren Te Ninove Doorn Noord. Analysis Report. RMI Geophysical Research Center of Dourbes, p. 12 (in Dutch).
- Stoneham, D., 1991. Authenticity testing. In: Göksu, H.Y., Oberhofer, M., Regula, D. (Eds.), *Scientific Dating Methods*. Kluwer Academic Publishers, pp. 175–192.
- Sun, Y.J., Chongyi, E., Lai, Z.P., Hou, G., 2018. Luminescence dating of prehistoric hearths in Northeast Qinghai Lake and its paleoclimatic implication. *Archaeological and Anthropological Sciences* 10, 1525–1534. <https://doi.org/10.1007/s12520-017-0472-y>.
- Sun, Y.J., Lai, Z.P., Madsen, D.B., Hou, G.L., 2012. Luminescence dating of a hearth from the archaeological site of Jiangxigou in the Qinghai Lake area of the northeastern Qinghai-Tibetan plateau. *Quat. Geochronol.* 12, 107–110. <https://doi.org/10.1016/j.quageo.2012.01.010>.
- Stuiver, M., 1961. Variations in radiocarbon concentration and sunspot activity. *Geophysical Research* 66, 273–276. <https://doi.org/10.1029/JZ066i001p00273>.
- Tans, P.P., De Jong, A.F.M., Mook, W.G., 1979. Natural atmospheric ^{14}C variation and the Suess effect. *Nature* 280, 826–828. <https://doi.org/10.1038/280826a0>.
- Vandenbergh, D., Kasse, C., Hossain, S.M., De Corte, F., Van Den Haute, P., Fuchs, M., Murray, A.S., 2004. Exploring the method of optical dating and comparison of optical and ^{14}C ages of Late Weichselian coversands in the southern Netherlands. *J. Quat. Sci.* 19, 73–86. <https://doi.org/10.1002/jqs.806>.
- Vandenbergh, D., De Corte, F., Buylaert, J.P., Kučera, J., Van den haute, P., 2008. On the internal radioactivity in quartz. *Radiat. Meas.* 43, 771–775. <https://doi.org/10.1016/j.radmeas.2008.01.016>.
- Verbrugge, A., Wauters, E., Cherretté, B., Poulain, M., Brion, M., 2022. Les campements militaires à Ninove (1667-1748): premiers résultats des fouilles archéologiques. The archaeology of conflicts : early modern military encampments and material culture. BAR International Series 3093 99–113. <http://hdl.handle.net/1854/LU-01GNAGM VY737XY9FDCB1VAAMMH>.
- Wagner, G.A., 1998. *Age determination of young rocks and artifacts: physical and chemical clocks in Quaternary geology and archaeology*. Springer-Verlag, Berlin Heidelberg. ISBN: 3-540-63436-3.
- Wang, C.X., Ji, X., Wu, Y., Jin, Z., Zhang, Y., Chen, M., Wang, N., Fan, A., 2022a. Quartz OSL and TL dating of pottery, burnt clay, and sediment from Beicun archaeological site, China. *Quat. Geochronol.* 70, 101281. <https://doi.org/10.1016/j.quageo.2022.101281>.
- Wang, C.-X., Zhang, X., Zhang, Y., Wu, Y., Huang, C., Fan, A., 2022b. Luminescence dating of heated quartz extracted from burnt clay and pottery excavated from the Lingjiantan archaeological site, China. *Front. Earth Sci.* 10, 933342. <https://doi.org/10.3389/feart.2022.933342>.
- Wauters, E., Verbrugge, A., 2022. Les campements militaires à Ninove (1667–1748): instruments de recherche et contexte historico-militaire. The archaeology of conflicts: early modern military encampments and material culture. BAR International Series 3093. <https://doi.org/10.30861/9781407359618>.
- Wintle, A.G., Murray, A.S., 1997. The relationship between quartz thermoluminescence, photo-transferred thermoluminescence and optically stimulated luminescence. *Radiat. Meas.* 27, 611–624. [https://doi.org/10.1016/S1350-4487\(97\)00018-8](https://doi.org/10.1016/S1350-4487(97)00018-8).
- Yu, L., An, P., Lai, Z.P., 2016. Different implications of OSL and radiocarbon ages in archaeological sites in the Qaidam Basin, Qinghai-Tibetan Plateau. *Geochronometria* 43, 188–200. <https://doi.org/10.1515/geochr-2015-0048>.